

Morphological considerations of the nickel chloride electrodes for zebra batteries

Jai Prakash^{a,*}, Laszlo Redey^b, Donald R. Vissers^b

^a Center for Electrochemical Science and Engineering, Department of Chemical and Environmental Engineering, Illinois Institute of Technology, Chicago, IL 60616, USA

^b Chemical Technology Division, Argonne National Laboratory, Argonne, IL 60439, USA

Received 18 February 1999; accepted 15 June 1999

Abstract

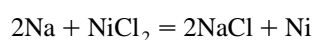
Electrochemical and morphological investigations of various nickel chloride electrodes were carried out. Three different types of Nickel chloride electrodes were investigated in this study: a nonporous nickel substrate, a nickel felt, and a porous sintered electrode. It was observed that the nickel chloride layer formation during the charge limits the area capacity of solid nickel to 0.6 C/cm^2 . There is also a direct relationship between the electrochemical performance and morphological parameters of the nickel chloride electrode. The capacity trend of these electrodes was explained by considering both the surface area and the pore-size distribution necessary for an effective mass transport during charge and discharge reactions. A rational approach to fabricate electrodes with improved nickel utilization is also discussed. © 1999 Elsevier Science S.A. All rights reserved.

Keywords: Zebra battery; Nickel chloride; Sodium; Sodium/nickel chloride cells; Morphology

1. Introduction

Zebra batteries based on Na/NiCl₂ chemistry offer many attractive properties: high cell voltage, high theoretical specific energy, broad range in operating temperature, and high reliability due to a failure mode that results in a hard short-circuit within the failed cell. This battery couple was originated in South Africa [1]. The Na/NiCl₂ cell is similar to the Na/S cell in that it uses much of the same technology. For instance, the Na/NiCl₂ cell, like the Na/S, uses a liquid sodium negative electrode and the β''-alumina solid electrolyte. However, unlike the sodium/sulfur cell, it uses a secondary electrolyte of molten sodium tetrachloroaluminate (Na[AlCl₄]) in the positive electrode and an insoluble nickel chloride as the active material. The Na[AlCl₄] electrolyte conducts sodium ions from the β''-Al₂O₃ electrolyte to the nickel chloride electrode reaction site. Sodium and Na[AlCl₄] are molten at the operational temperature (170 to 400°C) of the cell. Na[AlCl₄] is added to the porous Nickel chloride electrode

to transport Na⁺ ions from the surface of the β''-alumina electrolyte to the reaction sites at the interior of the positive electrode. The cell reaction is



In addition, this system also has several other advantages over other high temperature batteries such as Na/S and Li/FeS₂ batteries. These include compatibility of current collector and active material (contrast to Li/FeS₂ and Na/S cells), failure mechanism that short-circuits the cell (contrast to Na/S cells), good safety features and compatibility with the existing sodium-cell technology. In addition, the less corrosive nature of the NaAlCl₄ than sodium polysulfides used in the Na/Sulfur battery makes the selection of the hardware (cell container and current collectors) easier. Due to these excellent characteristics [2–9], these batteries are under intensive development in England, Germany, and Japan for electrically powered vehicles and load leveling electrical utilities. The performance of the present Na/NiCl₂ batteries, despite their high theoretical specific energy and cell voltage is limited due to the performance-limiting characteristics of the positive electrode [10]. The present state-of-art Na/Nickel chloride battery, has relatively high impedance, mainly in

* Corresponding author. Tel.: +1-312-567-3639; E-mail: prakash@charlie.cns.iit.edu

the positive electrode, because of its electrode kinetics, electrode morphology, and cell configuration. The nickel chloride electrode thus plays an important role in the resistance and weight of the cell; consequently, a quantitative understanding of the electrochemical and morphological properties of the NiCl_2 is very important.

The electrochemical behavior of Nickel chloride as the positive electrode in the Na/NiCl_2 cell has been extensively studied [10–20]. Most of these studies acknowledged that the cell performance is limited due to the NiCl_2 layer on the electrode which results in an area-capacity limit (ACL). The fundamental studies conducted on nonporous electrodes [17,20] suggest that a high surface area and an optimum pore-size distribution are essential for the development of a high-performance nickel electrode. However, a quantitative relationship between the morphological properties and the performance of the electrode has not been reported. This paper describes the fundamental electrochemical and morphological properties of the Nickel chloride electrode and a quantitative relationship between these properties and the electrode performance.

2. Experimental

Electrochemical investigations of the Na/NiCl_2 cell were carried out in an electrochemical research cell, which closely simulates the components and operational conditions of the full size battery. The capacity of these cells ranged between 0.6 to 1.2 Ah. The research cell had a molten sodium negative electrode, a nickel chloride positive electrode, a β'' -alumina tube (CSPL, U.K.) and a molten electrolyte, $\text{Na}[\text{AlCl}_4]$ (APL Engineered Materials). The molten sodium electrode also served as the reference electrode due to its negligible polarization. Three different types of Nickel chloride electrodes were investigated in this study; a nonporous nickel, a nickel felt, and a porous sintered nickel electrode. The electrodes were assembled in the discharged state by mixing of Ni-255 (Novamet Specialty Products) and NaCl powders (Aldrich Chemical) thoroughly and then pressing the material into a 0.5-cm thick pellet with a diameter of 2.80 cm. Both the nickel

felt and the sintered nickel electrode contained 15-vol.% nickel. The pellet was subsequently sintered at 750–890°C under a reducing atmosphere. Fabrication of the electrodes with nickel felt as the nickel matrix did not need the laborious and very delicate Ni powder sintering process. The commercial felts already had fine Ni powders sintered to the surface of the nickel fibers to increase the surface area (Fig. 4). The sintered felts were loaded with NaCl by either vibrating salt powder into the pores of the felt or evaporating salt solutions on the heated felt. Attachment of the felt to the current collector was carried out by spot welding on the current collector. The improved porous electrode (~ 1.2 Ah capacity) with better morphology was fabricated by mixing 4.29 g of Ni-255, 2.84 g of NaCl, and 0.713 g of ammonium bicarbonate as the poreformer (10 wt.% of the dry electrode) and then pressing the mixture into a 0.5-cm thick pellet with a diameter of 2.80 cm. This pellet was placed in a tube furnace and heated first at 250°C under a hydrogen containing atmosphere (5 wt.% hydrogen + 95% helium) for 1 h in order to decompose ammonium bicarbonate into NH_3 , CO_2 and H_2O vapors. The pellet was subsequently sintered at 750–890°C under a reducing atmosphere. After sintering, these electrodes were vacuum impregnated with liquid $\text{Na}[\text{AlCl}_4]$, and then placed in the cell's positive electrode compartment. The positive electrode compartment contained enough NaCl to saturate the liquid even during fully charged conditions. A uniform one-dimensional current distribution was maintained in the Nickel chloride electrode galvanostatically in the anodic (3.0 V) and cathodic (2.0 V) directions against a Na electrode. Current interruption technique was used during the cycling to evaluate the electrode and cell impedance.

The surface areas of the nickel specimens were determined by the BET N_2 gas adsorption method using a Quantasorb instrument (Quantachrome). The mercury porosimeter (Micromeritics) technique was used to obtain the pore-size distribution in the nickel samples. The surface-area, pore-size distribution, and SEM were carried out after the chloride salts had been leached from the electrodes.

Table 1
Electrode area and capacity parameters of Nickel chloride electrodes at 300°C in NaCl-saturated $\text{Na}[\text{AlCl}_4]$

	Nonporous nickel	Nickel felt	Sintered electrode
Observed capacity per geometric area, C/cm^2	0.6	130.2	720.0
Weight of Ni in the electrode, g		1.96	4.29
Measured volumetric capacity, C/cm^3	–	260	1440
BET area, m^2/g	–	0.3	1.8
Area factor ^a	1.0	957	12590
Calculated area capacity, C/cm^2	0.6 ^b	574	7554
Measured real area capacity, C/cm^2	0.6	0.136	0.057

^aThis factor is obtained by dividing the BET area by the geometrical area of the electrode.

^bThe value is for the geometrical area and may deviate due to the roughness factor.

3. Results and discussion

The BET areas of the nickel felt and the sintered electrode were found to be 0.3 and 1.8 m²/g, respectively and are reported in Table 1. It can be seen from this table that the sintered electrode fabricated with nickel powder has the maximum surface area. The geometrical area is used for the nonporous flat nickel electrode. From the BET area values, one can calculate an area factor, i.e., the real surface area per square centimeter of the geometrical area of these electrodes. These values are shown in Table 1. The pore-size distribution of the porous sintered electrode and the felt electrodes are shown in Figs. 1 and 2, respectively. These figures indicate that the felt and the sintered electrodes possess bimodal pore distribution. The median pore diameter in the nickel felt electrode is significantly greater than the median pore diameter in the sintered electrode.

The research cells used in this study simulate the components and mimic the operational conditions of a full-size Na/NiCl₂ cell. The electrodes fabricated with the nickel plate, nickel felt, and porous sintered electrodes possess different morphologies. Scanning electron micrographs showing the morphological characteristics of the sintered and the felt electrodes are shown in Figs. 3 and 4, respectively. Therefore, testing of these electrodes at identical conditions provides an opportunity to investigate the effect of the pore-size and the surface area on the electrode performance. Maintaining one-dimensional current density distribution in the Nickel chloride electrode, the charge and discharge capacities of the nickel chloride electrode can be precisely measured. The nickel utilization for porous

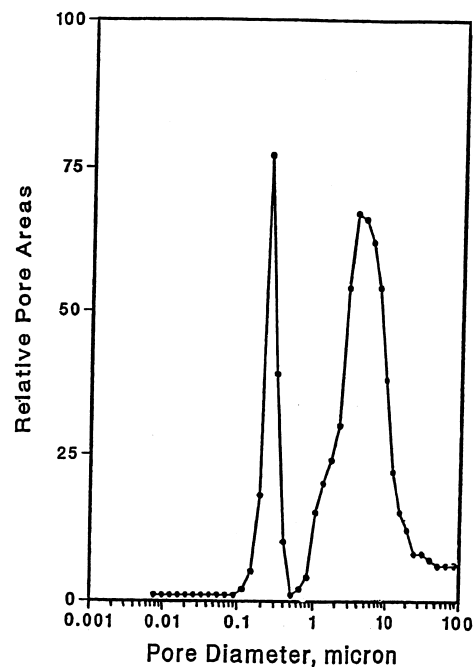


Fig. 2. Pore-size distribution of nickel chloride felt electrode.

nickel chloride electrodes was calculated on the basis of the ratio of the reacted NaCl and the total quantity of NaCl used to fabricate the positive electrode. This is because these cells are fabricated in the discharged state and the Nickel chloride active material is formed electrochemically during the charge reaction. The capacity achieved at the 10th cycle for the three nickel electrodes (nonporous, felt, and sintered) is used in the present discussion in order to

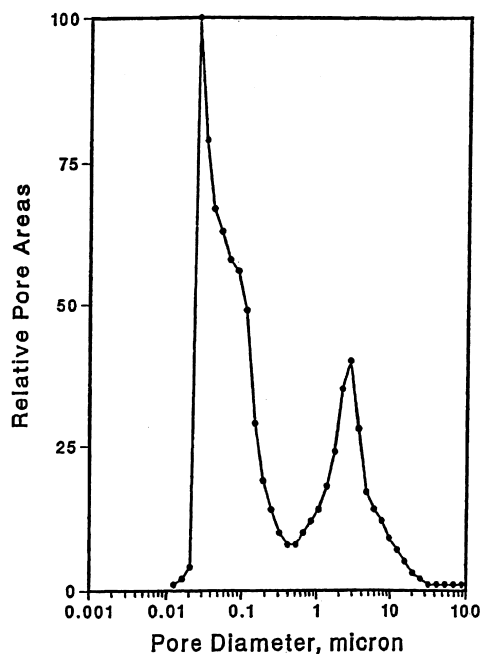


Fig. 1. Pore-size distribution of sintered nickel chloride electrode.

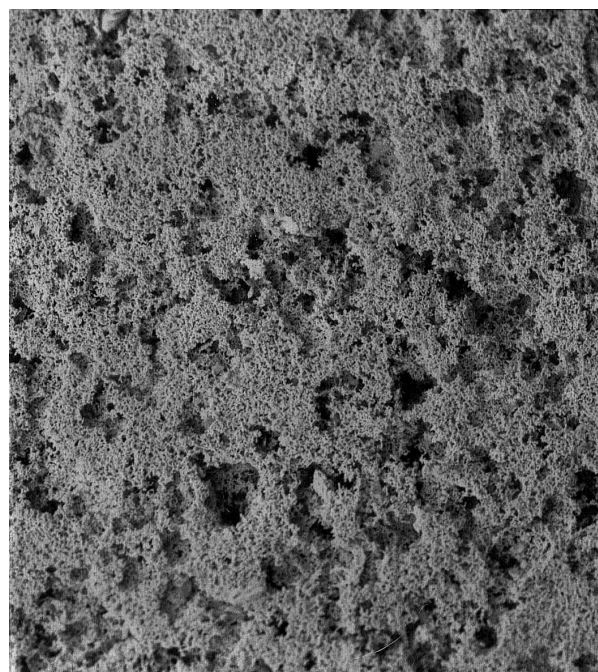


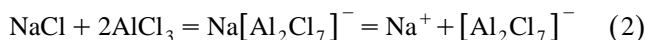
Fig. 3. Scanning Electron Micrographs of sintered nickel electrode.

avoid the complications associated with the capacity loss in the later cycles.

The $\text{Na}[\text{AlCl}_4]$ is a Lewis acid-base system and is characterized by the $\text{AlCl}_3/\text{NaCl}$ mole ratio. The mole percent of AlCl_3 can be easily adjusted by additions of small measured quantities of AlCl_3 to the NaCl -saturated melt of known weight. For example, the 1:1 ratio produces the neutral melt.



Ratios higher than 1:1 make acidic melts.



Basic melts such as the electrolyte used in Na/NiCl_2 cells, can be obtained at $\text{AlCl}_3:\text{NaCl}$ (excess NaCl than 1:1 ratio). NaCl is sparingly soluble in the basic melt. The NaCl -saturated basic melt has 49.75:51.25 $\text{AlCl}_3:\text{NaCl}$ ratio. The solubility of NiCl_2 in chloroaluminate melt is of critical importance in determining the cycle life of the Na/NiCl_2 cell. It has been shown [21] that a high concentration of free Ni^{2+} ions exists in the acidic chloroaluminate melt which can exchange with the Na^+ ions of the β'' -alumina, resulting in lowered conductivity and stability of the component of the Na/NiCl_2 cell. This exchange jeopardizes the β'' -alumina integrity and reduce the cell life-time. The basic melt, on the other hand, stabilizes the nickel in the complex-ion form $[\text{NiCl}_4]^{2-}$ form, reduces the concentration of the Ni^{2+} , and thus, hinders the deleterious ion exchange reaction. This fact clearly underlines

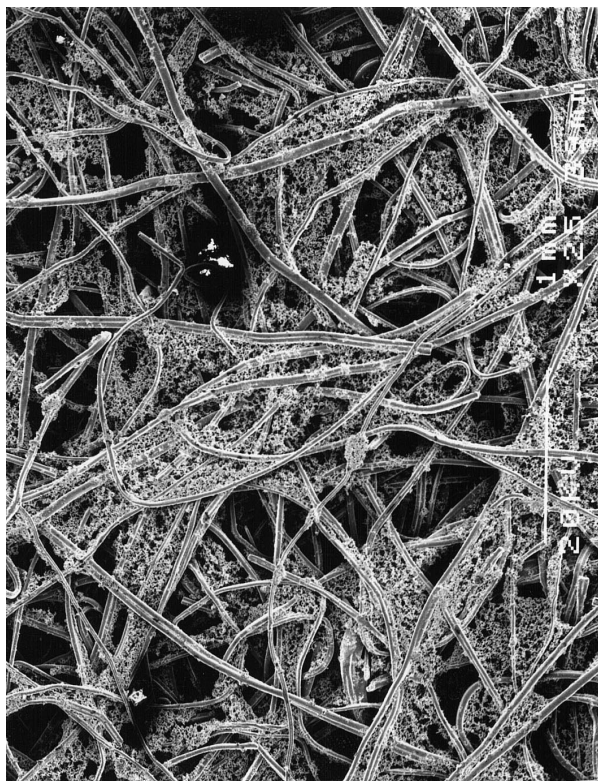


Fig. 4. Scanning Electron Micrographs of nickel felt electrode.

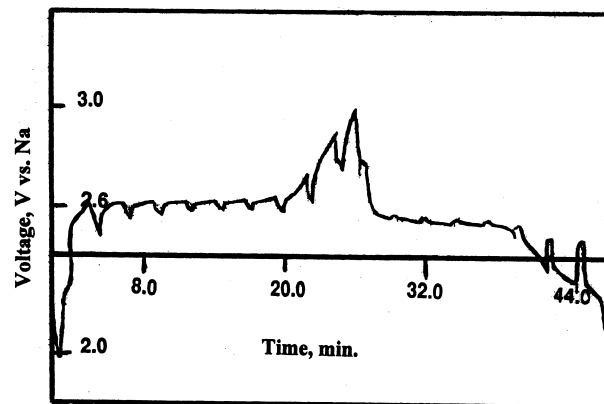


Fig. 5. Typical charge and discharge curves of a flat nonporous Nickel chloride electrode vs. Na in NaCl -saturated $\text{Na}[\text{AlCl}_4]$ melt at 300°C after the break-in cycles.

the importance of maintaining basic electrolyte in the Na/NiCl_2 cells. A buffered basic melt was maintained by having an excess solid NaCl in the Ni electrode all the time.

The Nickel chloride electrode gradually improves in the first 8–10 cycles and finally reaches a steady condition. The positive electrode made from flat nonporous nickel showed an improvement in the capacity in the few cycles before reaching a steady state. The increase in the capacity is attributed to the roughening of the electrode surface. Fig. 5 shows typical charge and discharge curves of a flat nonporous nickel electrode cycled between 2.0 and 3.0 V cell-voltage cut-offs vs. Na. It is clear from this figure that a wide potential range of cycling is required to fully utilize the electrode. Noteworthy is the break on the charge and discharge curves, which separates the half-cycles into two clearly distinguishable sections. For the nonporous nickel electrode, however, area capacity is used to express the utilization. The reason for this is because the electrolyte/Ni ratio in the nonporous electrode study is different from the one that prevails in a porous electrode structure. An interesting feature of the Nickel chloride electrode is the “self-limitation” of the available area capacity. The area-capacity limit ACL, the practically available capacity of the electrode per cm^2 area) is a strong function of current density and temperature. Area-capacity limits measured at different temperatures in NaCl saturated (basic) electrolyte are shown in Fig. 6. The area capacities shown in Fig. 6 were measured at $1 \text{ mA}/\text{cm}^2$ current density (equivalent to 3 to 10 min charge or discharge rates).

Figs. 7 and 8 show the charge and discharge capacities of the felt and sintered nickel chloride electrodes at C/10 rate cycled between 2.0 to 3.0 V. The porous sintered electrode showed a stable capacity from the second cycle onwards. The higher capacity of the sintered electrode is attributed to its higher electrochemical active area.

From the BET area values of various nickel electrodes, one can calculate an “area factor” i.e., the real surface

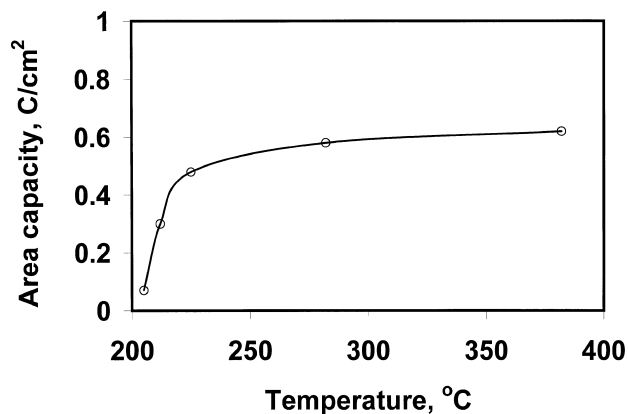


Fig. 6. Limiting area capacity of a nonporous nickel electrode.

area per square centimeter of the geometrical area of these electrodes. These values are also shown in Table 1. From the measurements carried out on the flat nonporous nickel electrodes, it was observed that one can obtain from 0.20 to 1.20 C/cm² on the nickel metal surface, depending on the experimental conditions. The area-capacity limit of 0.6 C/cm² however, is for the geometrical area of the electrode and might deviate if one assumes a roughness factor for the nickel. Multiplying the BET area of the electrode by the weight of nickel in the sintered electrode one can calculate the total real area of the nickel available in the electrode. The capacity per real area may then be calculated using the values of the real area. The capacities of the felt and porous sintered nickel chloride electrodes normalized to the geometrical areas (C/cm²) for these three electrodes are also given in Table 1.

Table 1 clearly shows a large difference between the calculated and the measured capacities values for the felt and the sintered electrode. This difference can be explained on the basis of the poorly conducting NiCl₂ layer formation during the charge reaction. The high resistance of this NiCl₂ layer inhibits the further thickening of the layer during charging of the nickel electrode. During the

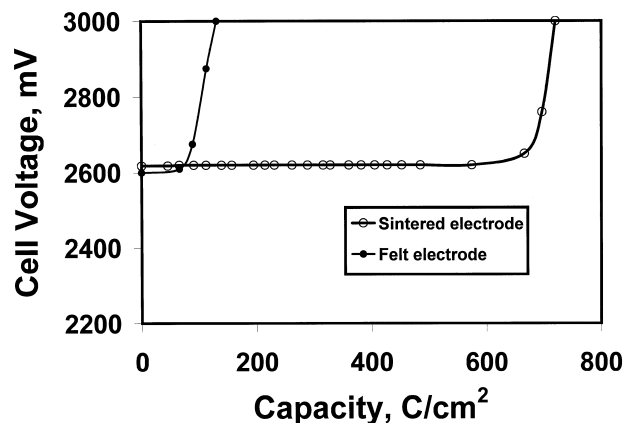


Fig. 7. Charge curves of the felt and the sintered Nickel chloride electrodes vs. Na in Na[AlCl₄] melt at 300°C and C/10 rate.

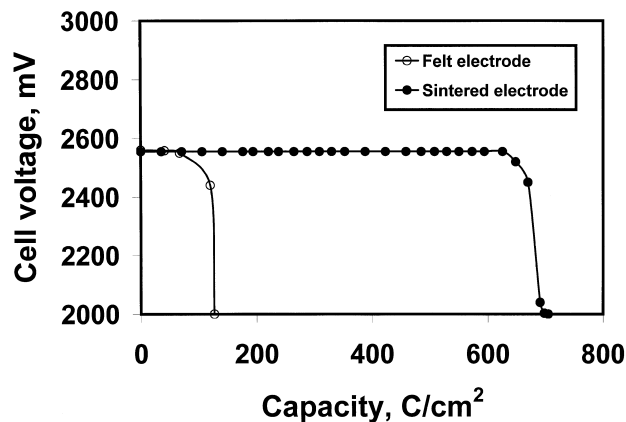


Fig. 8. Discharge curves of the felt and the sintered Nickel chloride electrodes vs. Na in Na[AlCl₄] melt at 300°C and C/10 rate.

discharge reaction, on the other hand, the formation of solid sodium chloride tends to cover the electrode surface and results in high resistance. Both these factors tend to limit both the energy and power characteristics of the nickel chloride electrode. Using the measured area capacity limit (ACL) of 0.6 C/cm², one can calculate 1.15 μm for the thickness of the NiCl₂ layer. This layer, once formed, would block the pores that have a radius smaller than the thickness of the layer. The results of the pore-size distribution studies carried out on the sintered electrode (Fig. 1) indicate that a majority of the pores in the sintered electrode lie below 3 μm. Therefore, the majority of these pores in the sintered electrode are filled with low-conducting nickel chloride, even during the early stage of charge.

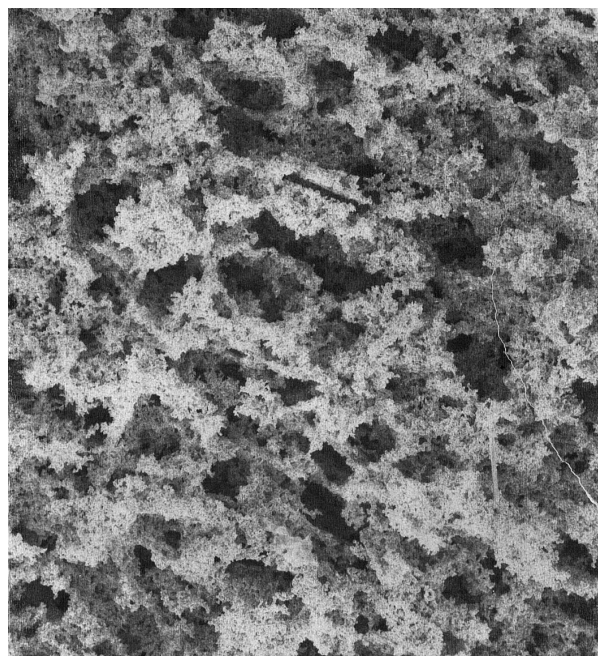


Fig. 9. Scanning Electron Micrographs of the nickel chloride electrode fabricated with poreformers.

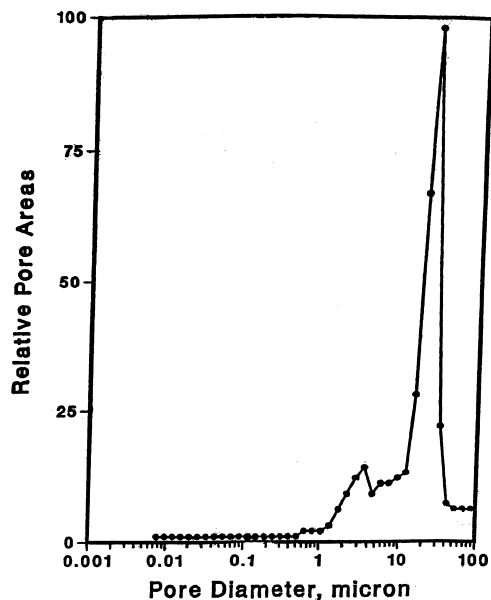


Fig. 10. Pore-size distribution of the nickel chloride electrode fabricated with poreformers.

This explains the difference of six orders of magnitude in the measured and calculated capacity of the sintered electrode. To utilize more nickel during the charge reaction, one would expect a NiCl_2 layer even thicker than $1.15 \mu\text{m}$. Based on Fig. 2 the felt electrode has pores that are $5 \mu\text{m}$ and, hence, are not completely blocked by the NiCl_2 during charge and NaCl during discharge reactions. Consequently, on the basis of real surface area and larger pore cavities, more nickel can be utilized in the case of the felt electrode. Therefore, it is critically important to improve the porosity of the electrode by providing pores larger than $1.15 \mu\text{m}$ to help mass transport during charge and discharge reactions.

These results show that it is critical to consider pore surface accessibility to calculate the capacity limit for a given pore-size distribution. These measurements also provide firm theoretical basis for the improvement of the

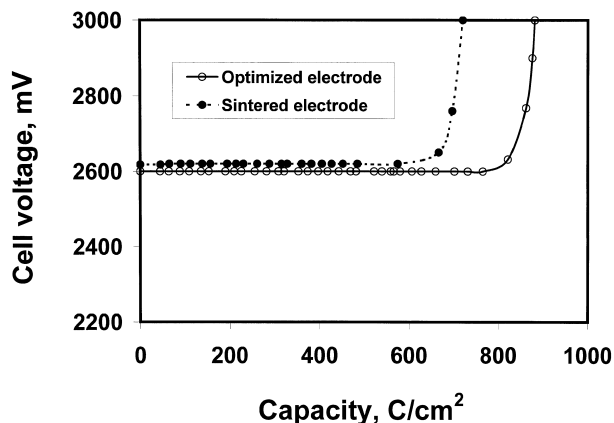


Fig. 11. Charge curves of the sintered and optimized Nickel chloride electrodes vs. Na in $\text{Na}[\text{AlCl}_4]$ melt at 300°C and $C/10$ rate.

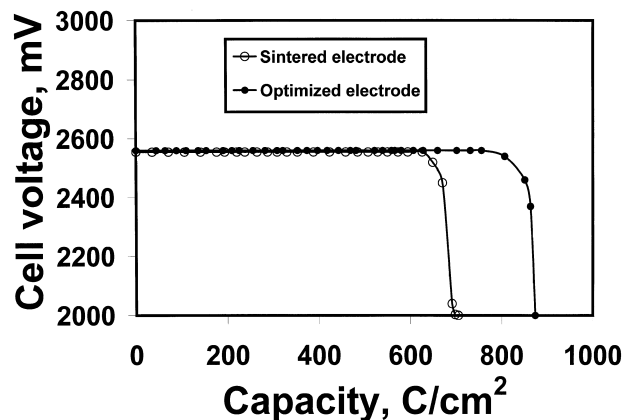


Fig. 12. Discharge curves of the sintered and optimized Nickel chloride electrodes vs. Na in $\text{Na}[\text{AlCl}_4]$ melt at 300°C and $C/10$ rate.

modified-morphology Nickel chloride electrodes. A porous nickel chloride electrode based on these morphological concepts would be expected to exhibit improved performance. Based on these principles, the morphology of a nickel chloride electrode was modified by the use of poreformers during fabrication step in order to attain controlled pore-size distribution. A scanning electron micrograph representing the optimized morphology of this electrode is shown in Fig. 9. The pore-size distribution of this electrode is also shown in Fig. 10. It can be seen from this figure that this electrode contains two types of pores. It contains pores that are about $2\text{--}10 \mu\text{m}$. In addition, it contains pores that are larger than $25 \mu\text{m}$. Smaller pores provide the high surface area and the large pores provide the pore cavities to support an effective mass transport during electrochemical reaction. Since the nickel chloride reaches to a thickness of about $1.15 \mu\text{m}$, the pores in this tailored electrode do not get blocked by the NiCl_2 during charge reaction. Also, the large pores can accommodate the NaCl crystals up to $25 \mu\text{m}$ during discharge reaction. Consequently, more active material can be utilized in the case of the morphologically tailored electrode. The electrochemical performance curves of a sintered electrode and a tailored electrode with an optimized morphology are shown in Figs. 11 and 12. The superior performance of the tailored nickel chloride electrode fabricated with the poreformer is clearly indicated by the extended cell capacity. This can be explained on the basis of improved morphology of the tailored nickel chloride electrode provided by the high surface area and sufficient optimized pore cavities to support an effective mass transport during charge and discharge reactions.

4. Conclusion

These experiments have proven that NiCl_2 layer formation during charge limits the area capacity in Nickel chloride electrodes. There is a direct relationship between

the electrochemical performance and the morphological properties (BET area and pore-size distribution) of the electrode. It is, therefore, critical to consider both the surface area and the pore surface accessibility to estimate the capacity limit for a given pore-size distribution. These investigations also provide firm theoretical basis for the improvement of the modified-morphology Nickel chloride electrodes. A porous electrode with a specially tailored morphology produces an improved performance by providing high surface area and sufficient pore cavities to support effective mass transport.

Acknowledgements

The work described here was carried out at the Chemical Technology Division of the Argonne National Laboratory. The authors are grateful to Dr. Kenneth Heitner of the Office of Transportation Systems, Electric and Hybrid Propulsion Division, U.S. Department of Energy. This work was supported by the Department of Energy under contract No. W-31-109-Eng. 38.

References

- [1] J. Coetzer, *J. Power Sources* 18 (1986) 377.
- [2] J. Coetzer, R.J. Bones, R.C. Galloway, D.A. Teagle, P.T. Moseley, U.S. Pat. 4,546,055, 1985.
- [3] R.C. Galloway, *J. Electrochem. Soc.* 134 (1987) 256.
- [4] R.J. Bones, J. Coetzer, R.C. Galloway, D.A. Teagle, *J. Electrochem. Soc.* 134 (1987) 2379.
- [5] R.J. Wedlake, A.R. Tilley, D.A. Teagle, *Bull. Electrochem.* 4 (1988) 41.
- [6] R.M. Dell, R.J. Bones, *Bull. Electrochem.* 4 (1988) 319.
- [7] J. Sudworth, *Chem. Ind.* 1 (1988) 77.
- [8] P.T. Moseley, R.J. Bones, D.A. Teagle, B.A. Bellamy, R.W.M. Hawes, *J. Electrochem. Soc.* 136 (1989) 1361.
- [9] R.J. Bones, D.A. Teagle, S.D. Brooker, F.L. Cullen, *J. Electrochem. Soc.* 136 (1989) 1274.
- [10] L. Redey, D.R. Vissers, J. Prakash, U.S. Patent No. 5,283,135, 1994.
- [11] L. Redey, D.R. Vissers, J. Prakash, U.S. Patent No. 5,340,668, 1994.
- [12] L. Redey, D.R. Vissers, J. Prakash, K.M. Myles, U.S. Patent No. 5,532,078, 1996.
- [13] L. Redey, D.R. Vissers, J. Prakash, K.M. Myles, U.S. Patent No. 5,536,593, 1996.
- [14] B.V. Ratnakumar, S. Di Stefano, G. Halpert, *J. Electrochem. Soc.* 137 (1990) 2991.
- [15] L. Redey, J. Prakash, D.R. Vissers, K.M. Myles, *Proc. of 35th International Power Sources Symp.*, Cherry Hill, NJ, June 22–25, 1992.
- [16] J. Prakash, L. Redey, D.R. Vissers, *Extended Abstracts, Electrochemical Society Meeting, Toronto, Canada, October 11–16, 1992.*
- [17] L. Redey, D.R. Vissers, *Extended Abstracts, Electrochemical Society Meeting, Hollywood, FL, October 15–20, 1989.*
- [18] R.J. Bones, J. Coetzer, R.C. Galloway, D.A. Teagle, *J. Electrochem. Soc.* 134 (1987) 2370.
- [19] L. Redey, D.R. Vissers, *Extended Abstracts, Electrochemical Society Meeting, Hollywood, FL, October 15–20, 1989.*
- [20] J. Prakash, L. Redey, D.R. Vissers, *Extended Abstracts, Electrochemical Society Meeting, Washington, DC, May 5–10, 1991.*
- [21] L. Redey, C. Rose, R. Lowrey, *Extended Abstracts, Electrochemical Society Meeting, Toronto, Canada, 1992, p. 116.*